

Force Profiling of a Shoulder Bidirectional Fabric-based Pneumatic Actuator for a Pediatric Exosuit

Mehrnoosh Ayazi,¹ Ipsita Sahin,² Caio Mucchiani,¹ Elena Kokkoni,² and Konstantinos Karydis¹

Abstract—This paper presents a comprehensive analysis of the contact force profile of a single-cell bidirectional soft pneumatic actuator, specifically designed to aid in the abduction and adduction of the shoulder for pediatric exosuits. The actuator was embedded in an infant-scale test rig featuring two degrees of freedom: an actuated revolute joint supporting shoulder abduction/adduction and a passive (but lockable) revolute joint supporting elbow flexion/extension. Integrated load cells and an encoder within the rig were used to measure the force applied by the actuator and the shoulder joint angle, respectively. The actuator’s performance was evaluated under various anchoring points and elbow joint angles. Experimental results demonstrate that optimal performance, characterized by maximum range of motion and minimal force applied on the torso and upper arm, can be achieved when the actuator is anchored at two-thirds the length of the upper arm, with the elbow joint positioned at a 90-degree angle. The force versus pressure and joint angle graphs reveal nonlinear and hysteresis behaviors. The findings of this study yield insights about optimal anchoring points and elbow angles to minimize exerted forces without reducing the range of motion.

I. INTRODUCTION

Fabric-based pneumatic actuators [1], [2] have been integrated into soft robotic devices for assistance and rehabilitation. Such devices consider a range of applications including lower limb [3], hip [4], and upper limb [5]–[8] support, grasping [9], [10], supernumerary robotic limbs [11], and haptics [12], [13]. Yet, existing efforts have mostly focused on adults [14], [15]. Only a few have considered developing devices to support upper-extremity (UE) movement in very young children [16]–[18].

To ensure comfortable and safe interaction between the user and the device, it is crucial to understand the exerted forces. Exerted forces can be determined based on the device’s mechanical components and affordances, such as actuator deformation as a function of input pressure [14] and anchoring [19]. Desired values for these forces are determined based on the users’ needs and tolerances [20]. Previous studies have focused on determining desired values to support motion about different joints and then developing adult devices capable of generating such forces. For example, the average peak torque requirement produced by a healthy deltoid muscle to completely elevate the arm was found to be 43 Nm [21]. To reach maximum arm elevation, a force of at

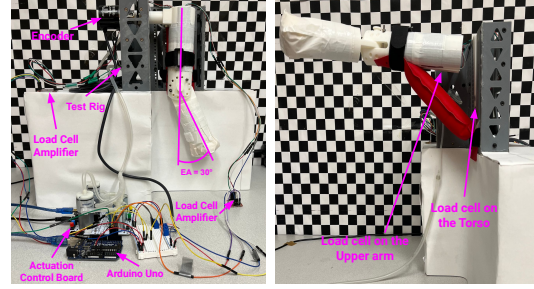


Fig. 1. Experimental setup employed in this work for force profiling of a fabric-based pneumatic shoulder actuator when the actuator anchoring points and elbow (locked in place) angle vary.

least 270 N must be generated [22]. Based on this analysis, a soft wearable deltoid assistance device [22] was developed to produce about 300 N force on the upper arm to elevate the arm to 90°. An exomuscle [14] can exert forces on the arm in the range of [0 – 500] N with varying actuator inflating pressure and shoulder abduction angle while testing on a one-degree-freedom apparatus. Other studies like a soft shoulder assistive device with pneumatic artificial muscles [23] and a cable-driven soft orthotic device [24] have targeted the generation of a maximum force output of approximately 100 N, which is similar to the compressive force generated by biological anterior deltoid muscle. Despite these findings, there have been no studies so far on the forces exerted by actuators or soft wearable UE devices on the infant body.

Our prior work has focused on the design and kinematics of actuators to support UE movement in very young children [25], [26], as well as on the development of feedback control methods for exosuit prototypes employing those actuators tested with an engineered mannequin [27], [28]. In this work, we study the force generation of our previously developed fabric-based pneumatic shoulder actuator using a static testing rig (Fig. 1). We vary two key conditions—anchoring points of the actuator on the torso and upper arm, and elbow joint angle—and observe how the exerted force and range of motion are affected. The goal is to identify which conditions can lead to minimal exerted forces and maximal range of motion. This information, in turn, can help pinpoint how to improve the exosuit’s functionality.

II. MATERIALS AND METHODS

A. Actuator Description

The soft pneumatic actuator used in this study was a rectangular-shaped, single-cell actuator, crafted from flexible thermoplastic polyurethane (TPU) fabric (Oxford 200D heat-sealable coated fabric with a thickness of 0.020 cm). The

¹ Dept. of Electrical and Computer Engineering; ² Dept. of Bioengineering, University of California, Riverside, 900 University Ave, Riverside, CA 92521, USA. Email: {mayaz004, isahi001, caiocesr, elenak, karydis}@ucr.edu. We gratefully acknowledge the support of NSF # CMMI-2133084. Any opinions, findings, and conclusions or recommendations expressed in this material are those of the authors and do not necessarily reflect the views of the National Science Foundation.

inflatable portion of the actuator is 15×5 cm. Two non-inflatable segments of about 3×5 cm at each end are used to facilitate attachment to the torso and upper arm using velcro straps. This actuator can support shoulder abduction and adduction without impeding other degrees of freedom (DoFs) at the joint by being placed in a low-profile position within the axilla. Among various actuators evaluated for shoulder assistance [25], this variant was selected based on rigorous criteria, with a primary focus on range of motion (ROM).

B. Hardware Experimentation Setup

We developed a 3D-printed test rig modeled based on the UE of the 50th percentile of a 12-month-old infant [29], [30] (Fig. 1). The rig comprises a base (torso), an upper arm, a forearm, and a weighted attachment (0.06 kg) at the end of the forearm to emulate the hand. The upper arm is connected to the base via a revolute joint acting as the shoulder joint. The forearm is connected to the upper arm through another revolute joint, acting as the elbow joint, which can be locked in place at four distinct angles ($EA \in \{0^\circ, 30^\circ, 60^\circ, 90^\circ\}$). The upper arm measures 16.4 cm in length and 14.7 cm in circumference, while the forearm measures 10.85 cm in length and 14.51 cm in circumference. Both the upper arm and forearm are hollow, and sandbags were embedded within to match the weight of an infant's upper arm and forearm (total weight about 0.432 kg), based on the infant anthropometrics for a total body mass of 10.8 kg [31].

Actuator inflation/deflation was controlled by an external pneumatic board (Programmable-Air kit). The board has two compressor/vacuum pumps and three pneumatic valves to regulate airflow (2 L/min). Airflow is adjusted via the pump duty cycle ($[0-100]\%$). The pressure range is $[-50, 50]$ kPa. The board also incorporates a pressure sensor (SMPP-03) and an Arduino Nano (ATMega328P) for control and monitoring. The embedded Arduino facilitates connectivity to a computer through a serial-to-USB interface, allowing users to send commands to the pumps and valves, and log sensor data.

The developed force measurement system consisted of two 5 kg load cells (YZC-133) embedded in the upper arm and base of the test rig. The upper arm load cell was positioned along the vertical centerline on the inner side of the upper arm. A plate measuring 11.1×1.36 cm was attached to the load cell to measure the force applied to the area covered by the plate. The load cell on the base was aligned with the vertical centerline on the side facing the inner side of the upper arm and was coupled with a 15.6×1.66 cm plate. Each load cell was connected to an amplifier (HX711, Sparkfun); data were read at a frequency of 10 Hz. A 1024 pulse per rotation rotary encoder (E6B2, Sparkfun) was used to measure the angle of the shoulder joint throughout the experiments. The amplified outputs of load cells and the encoder's data were transmitted to a computer through another microcontroller (Arduino UNO).

C. Experimental Conditions

The performance of the actuator in terms of force exerted on the upper arm and torso was assessed within a total of

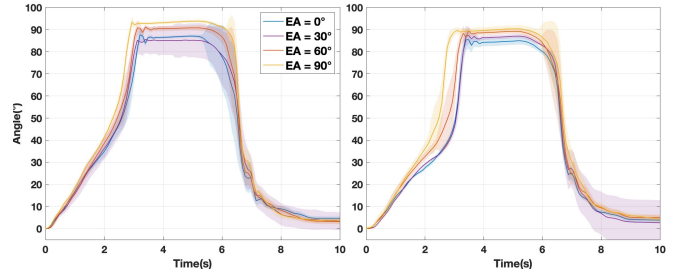


Fig. 2. Changes in shoulder joint angle over time where shaded area represents standard deviation. The panels at left and right represent anchoring at $\frac{2}{3}$ and $\frac{1}{2}$ the length of the upper arm, respectively.

eight different conditions varying based on the upper arm anchoring point and the locked elbow angle (Table I). A total of 30 trials were conducted for each condition. The actuation control board was operating at a 100% duty cycle to achieve the fastest possible inflation and deflation. A complete reaching motion in infants lasts about two seconds [32]; hence, we assessed both inflation and deflation phases each lasting for 5 seconds, starting with inflation. Internal actuator pressure peaked at a maximum of 34 kPa and dropped to a minimum of -34 kPa when fully inflated and deflated, respectively.

TABLE I

EXPERIMENTAL CONDITIONS

Anchoring Point	Elbow Angle
$\frac{2}{3}$ length of UA	$0^\circ, 30^\circ, 60^\circ, 90^\circ$
$\frac{1}{2}$ length of UA	$0^\circ, 30^\circ, 60^\circ, 90^\circ$

III. RESULTS AND DISCUSSION

A. Assessment of Shoulder Joint ROM

We first assessed shoulder joint ROM under the different conditions listed in Table I. It can be observed (Fig. 2) that increasing the elbow joint angle (i.e. flexing the elbow) results in a larger maximum shoulder joint angle as well as increased ROM. During elbow flexion, there is a reduction of the moment arm between the point where the mass at the end of the forearm is located and the shoulder joint axis of rotation. Less mechanical work is thus required but the amount of input pressure remains the same, which leads to larger ROM. Further, the shoulder joint has larger ROM when the actuator is anchored at $\frac{2}{3}$ the UA length. The moment arm between the actuator force location on the upper arm and shoulder joint increases when the placement of the actuator moves from half to two-thirds of UA length. Consequently, the actuator generates more torque with the same actuator pressure and force on the upper arm.

B. Assessment of Actuator Force Generation

We then examined the variation in the force exerted by the actuator on the torso and upper arm. Generally, the maximum (on average) force applied to the torso and upper arm decreases as the elbow joint angle increases (Fig. 3). However, this trend is not observed across all cases. The peak force on the torso and upper arm is created by the interaction between two segments of the actuator, which apply force to these areas. As the elbow flexes and the

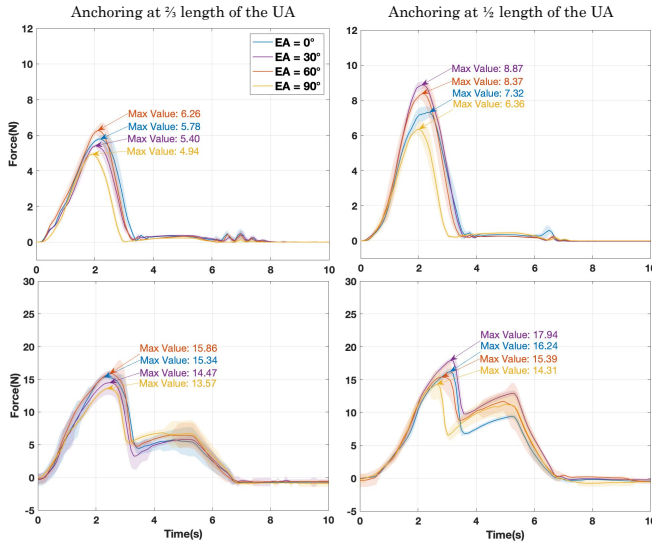


Fig. 3. Forces applied by the actuator on the torso (Top) and upper arm (UA) (Bottom) for the different experimental conditions listed in Table I. Shaded zones reflect one standard deviation (30 trials for each condition).

moment of inertia decreases, the interaction force between the segments decreases, thus reducing the maximum force applied to both the upper arm and torso. Further, when comparing peak forces between the two anchoring points, a notable trend emerges: while the force on the torso increases, the force on the upper arm stays relatively consistent. As the anchoring point shifts from two-thirds to half the length of UA, the area covered by the actuator on the torso expands which results in a larger force applied to the torso with the same actuator inner pressure. Since the actuator maintains the same coverage area on the upper arm in both scenarios, the maximum force exerted on the upper arm does not change.

The decline in force on both the upper arm and torso during actuator inflation can be associated with varying contacts during the process. Placed under the armpit, a single-cell actuator naturally folds, creating two distinct sections that effectively function as two separate cells until a critical point when they merge. These sections interact by pushing outward while inflating, increasing force on both the torso and upper arm. Around halfway through inflation, these sections merge into a single cell (crucial for maximizing ROM). However, this merging leads to a notable decrease in contact with both the upper arm and torso. Consequently, force at both points decreases abruptly. After unfolding, the actuator remains attached to the torso at its non-inflatable end, causing the force measured at the torso to drop nearly to zero. The force on the upper arm also declines but at a smaller degree since the inflatable part of the actuator still partially covers the upper arm. Hence, the force at the upper arm increases until the end of the inflation period. During deflation, the upper arm force decreases while the torso force remains near zero.

We also analyzed the relation between the forces exerted on the upper arm and torso and the actuator's internal pressure. The forces were found to be nonlinear and exhibit hysteresis as the input pressure varied (Fig. 4). For pressures below 10 kPa, the relation is linear; however, around 10 kPa, the actuator begins to unfold and a notable drop occurred

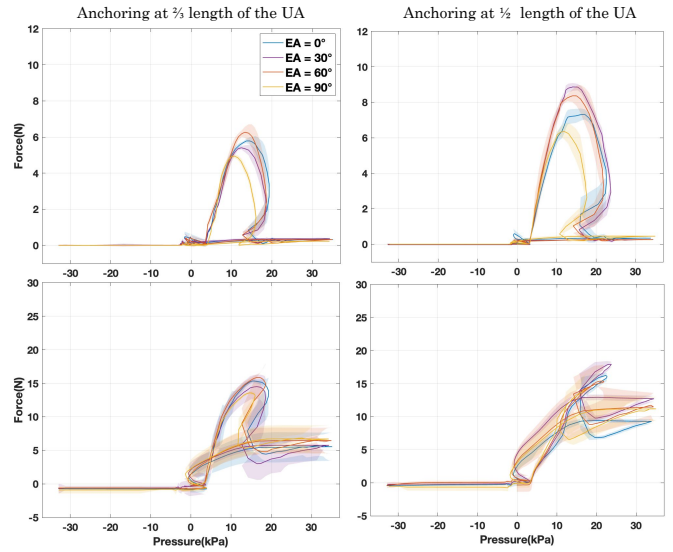


Fig. 4. Actuator force changes on the torso (Top) and upper arm (Bottom) as the internal pressure of the actuator varies.

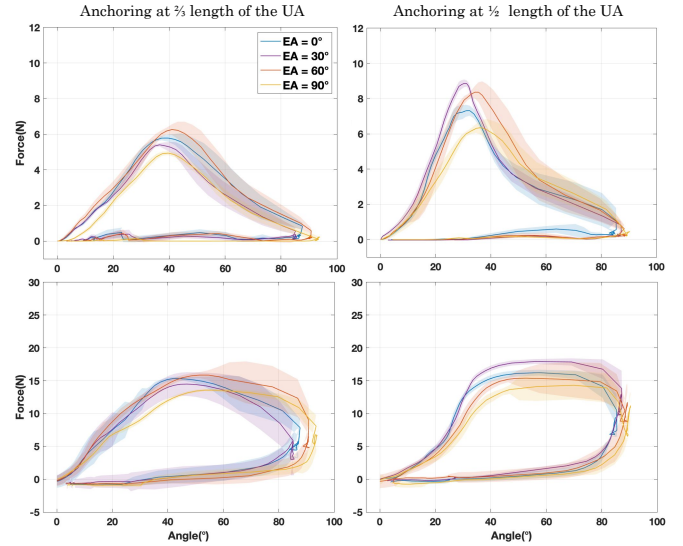


Fig. 5. Actuator force changes on the torso (Top) and upper arm (Bottom) as the shoulder joint angle increases.

because of the reduction in the contact area. The actuator pressure also decreases, likely due to the suddenly increased volume from the actuator unfolding. After this point, the force on the torso remains unchanged while the force on the upper arm starts to increase linearly with pressure. During deflation, the force on the torso is constant, whereas the force on the upper arm decreases roughly logarithmically.

Further, we analyzed the relation between exerted force and shoulder joint angle (Fig. 5). There is a major change when at about half the ROM, marking the point where the actuator begins to unfold. Identifying this angle as the threshold for actuator unfolding, we found that the force behavior aligns with the patterns described previously. Nonlinearity and hysteresis were observed here as well.

The maximum force generated by the actuator in this work is significantly lower compared to those developed for adult shoulder abduction/adduction [14], [22] which are at the range of [300 – 500] N. Although a direct comparison of absolute values may not be appropriate, this information

may help suggest upper bounds for exerted forces via a mechanics-based scaling. Such an assessment merits further investigation considering that there is limited information in the literature regarding the maximum forces that are safe to exert on infants' arms in the context of pediatric exosuits.

IV. CONCLUSION

This study examined the contact forces generated by a single-cell bidirectional soft pneumatic actuator for shoulder abduction/adduction using an infant-scale test rig. Extensive experimentation across different conditions related to actuator anchoring and (fixed) elbow joint angle demonstrated the optimal performance range of the considered actuator: the maximum range of motion while exerting minimal force on the torso and upper arm is achieved when anchored at two-thirds the length of the upper arm when the elbow joint is at a 90° angle. Nonlinearity and hysteresis between actuator input pressure, shoulder joint angle, and the exerted forces were identified. These were caused by the actuator's rapid unfolding during actuation, thereby suggesting future design improvements to produce smoother force profiles.

REFERENCES

- [1] A. Bhat, S. S. Jaipurkar, L. T. Low, and R. C.-H. Yeow, "Reconfigurable soft pneumatic actuators using extensible fabric-based skins," *Soft Robot.*, vol. 10, no. 5, pp. 923–936, 2023.
- [2] Z. Zhang, Y. Long, G. Chen, Q. Wu, H. Wang, and H. Jiang, "Soft and lightweight fabric enables powerful and high-range pneumatic actuation," *Sci. Adv.*, vol. 9, no. 15, p. 1203, 2023.
- [3] P. B. Banyarani, B. Tarvirdizadeh, and A. Hadi, "Design and fabrication of a soft wearable robot using a novel pleated fabric pneumatic artificial muscle (ppfam) to assist walking," *Sens. Actuators A. Phys.*, vol. 370, p. 115278, 2024.
- [4] T. M. Miller-Jackson, R. F. Natividad, D. Y. L. Lim, L. Hernandez-Barraza, J. W. Ambrose, and R. C.-H. Yeow, "A wearable soft robotic exoskeleton for hip flexion rehabilitation," *Front. Robot. AI*, vol. 9, p. 835237, 2022.
- [5] M. Xiloyannis, D. Chiaradia, A. Frisoli, and L. Masia, "Physiological and kinematic effects of a soft exosuit on arm movements," *J. Neuroeng. Rehabil.*, vol. 16, pp. 1–15, 2019.
- [6] F. Missiroli, N. Lotti, E. Tricomi, C. Bokranz, R. Alicea, M. Xiloyannis, J. Krzywinski, S. Crea, N. Vitiello, and L. Masia, "Rigid, soft, passive, and active: A hybrid occupational exoskeleton for bimanual multijoint assistance," *IEEE Robot. Autom. Lett.*, vol. 7, no. 2, pp. 2557–2564, 2022.
- [7] K. Schäffer, Y. Ozkan-Aydin, and M. M. Coad, "Soft wrist exosuit actuated by fabric pneumatic artificial muscles," *IEEE Trans. Med. Robot. Bionics*, pp. 718–732, 2024.
- [8] L. Cappello, J. T. Meyer, K. C. Galloway, J. D. Peisner, R. Granberry, D. A. Wagner, S. Engelhardt, S. Paganoni, and C. J. Walsh, "Assisting hand function after spinal cord injury with a fabric-based soft robotic glove," *J. Neuroeng. Rehabil.*, vol. 15, pp. 1–10, 2018.
- [9] J. H. Low, N. Cheng, P. Khin, N. V. Thakor, S. L. Kukreja, H. Ren, and C.-H. Yeow, "A bidirectional soft pneumatic fabric-based actuator for grasping applications," in *IEEE/RSJ Int. Conf. Intell. Robots Syst. (IROS)*, 2017, pp. 1180–1186.
- [10] P. H. Nguyen, S. Sridar, S. Amatya, C. M. Thalman, and P. Polygerinos, "Fabric-based soft grippers capable of selective distributed bending for assistance of daily living tasks," in *IEEE Int. Conf. Soft Robot. (RoboSoft)*, 2019, pp. 404–409.
- [11] P. H. Nguyen, I. I. Mohd, C. Sparks, F. L. Arellano, W. Zhang, and P. Polygerinos, "Fabric soft poly-limbs for physical assistance of daily living tasks," in *IEEE Int. Conf. Robot. Autom. (ICRA)*, 2019, pp. 8429–8435.
- [12] P. M. Khin, J. H. Low, W. W. Lee, S. L. Kukreja, H. Ren, N. V. Thakor, and C.-H. Yeow, "Soft haptics using soft actuator and soft sensor," in *IEEE-RAS EMBS Int. Conf. Biomed. Robot. Biomechatron.*, 2016, pp. 1272–1276.
- [13] M. Zhu, A. H. Memar, A. Gupta, M. Samad, P. Agarwal, Y. Visell, S. J. Keller, and N. Colonnese, "Pneusleeve: In-fabric multimodal actuation and sensing in a soft, compact, and expressive haptic sleeve," in *CHI Conf. Human Factors Comput. Syst.*, 2020, pp. 1–12.
- [14] C. S. Simpson, A. M. Okamura, and E. W. Hawkes, "Exomuscle: An inflatable device for shoulder abduction support," in *IEEE Int. Conf. Robot. Autom. (ICRA)*, 2017, pp. 6651–6657.
- [15] C. Simpson, B. Huerta, S. Sketch, M. Lansberg, E. Hawkes, and A. Okamura, "Upper extremity exomuscle for shoulder abduction support," *IEEE Trans. Med. Robot. Bionics*, vol. 2, no. 3, pp. 474–484, 2020.
- [16] B. Li, B. Greenspan, T. Mascitelli, M. Raccuglia, K. Denner, R. Duda, and M. A. Lobo, "Design of the Playskin Air™: A User-Controlled, Soft Pneumatic Exoskeleton," in *Des. Med. Dev. Conf.*, 2019, pp. 1–4.
- [17] A. J. Arnold, J. L. Haworth, V. O. Moran, A. Abulhasan, N. Steinbuch, and E. Kokkonis, "Exploring the unmet need for technology to promote motor ability in children younger than 5 years of age: a systematic review," *Arch. Rehabil. Res. Clin. Transl.*, vol. 2, no. 2, p. 100051, 2020.
- [18] E. Kokkonis, Z. Liu, and K. Karydis, "Development of a soft robotic wearable device to assist infant reaching," *J. Eng. Sci. Med. Diagn. Ther.*, vol. 3, no. 2, 2020.
- [19] W. Wei, Z. Qu, W. Wang, P. Zhang, F. Hao *et al.*, "Design on the bowden cable-driven upper limb soft exoskeleton," *Appl. Bionics Biomech.*, 2018.
- [20] A. Vega Ramirez and Y. Kurita, "A soft exoskeleton jacket with pneumatic gel muscles for human motion interaction," in *Universal Access in Human-Computer Interaction. Multimodality and Assistive Environments*. Springer International Publishing, 2019, pp. 587–603.
- [21] J. M. De Toledo, R. C. Krug, M. P. Castro, D. C. Ribeiro, and J. F. Loss, "Torque and force production during shoulder external rotation: differences between transverse and sagittal planes," *J. Appl. Biomech.*, vol. 24, no. 1, pp. 51–57, 2008.
- [22] F. J. L. Arellano, S. Gandhi, D. Patil, B. Roquemore, T. Maruyama, and P. Polygerinos, "Soft wearable deltoid assistive device," in *Des. Med. Devices Conf.*, vol. 41037. ASME, 2019.
- [23] S. Sridar, R. G. Narasimha, A. M. Gadagi, V. Taduru, C. Strzelczyk, T. Maruyama, C. StClair, and P. Polygerinos, "Soft robotic shoulder assist device: Towards prevention of shoulder overuse syndrome in wheelchair users," *Proc. Des. Med. Devices Conf.*, vol. 40789, 2018.
- [24] S. B. Kesner, L. Jentoft, F. L. Hammond, R. D. Howe, and M. Popovic, "Design considerations for an active soft orthotic system for shoulder rehabilitation," in *Annu. Int. Conf. IEEE Eng. Med. Biol. Soc.*, 2011, pp. 8130–8134.
- [25] I. Sahin, J. Dube, C. Mucchiani, K. Karydis, and E. Kokkonis, "A bidirectional fabric-based pneumatic actuator for the infant shoulder: Design and comparative kinematic analysis," in *IEEE Int. Conf. Robot & Human Inter. Comm. (ROMAN)*, 2022, pp. 371–376.
- [26] I. Sahin, M. Ayazi, C. Mucchiani, J. Dube, K. Karydis, and E. Kokkonis, "A fabric-based pneumatic actuator for the infant elbow: Design and comparative kinematic analysis," in *IEEE Int. Conf. Robot. Biom. (ROBIO)*, 2023, pp. 1–6.
- [27] C. Mucchiani, Z. Liu, I. Sahin, J. Dube, L. Vu, E. Kokkonis, and K. Karydis, "Closed-loop position control of a pediatric soft robotic wearable device for upper extremity assistance," in *IEEE Int. Conf. Robot & Human Inter. Comm. (ROMAN)*, 2022, pp. 1514–1519.
- [28] C. Mucchiani, Z. Liu, I. Sahin, E. Kokkonis, and K. Karydis, "Robust generalized proportional integral control for trajectory tracking of soft actuators in a pediatric wearable assistive device," in *IEEE/RSJ Int. Conf. Intell. Robots Syst. (IROS)*, 2023, pp. 559–566.
- [29] T. Edmond, A. Laps, A. L. Case, N. O'Hara, and J. M. Abzug, "Normal ranges of upper extremity length, circumference, and rate of growth in the pediatric population," *Hand*, vol. 15, no. 5, pp. 713–721, 2020.
- [30] C. D. Fryar, M. D. Carroll, Q. Gu, J. Afful, and C. L. Ogden, "Anthropometric reference data for children and adults: United states, 2015–2018," *Vital Health Stat.* 3, 2021.
- [31] K. Schneide and R. F. Zernicke, "Mass, center of mass, and moment of inertia estimates for infant limb segments," *J. Biomech.*, vol. 25, no. 2, pp. 154–148, 1992.
- [32] J. Zhou and B. A. Smith, "Infant reaching in the first year of life: A scoping review of typical development and examples of atypical development," *Phys. Occup. Ther. Pediatr.*, vol. 42, no. 1, pp. 80–98, 2021.